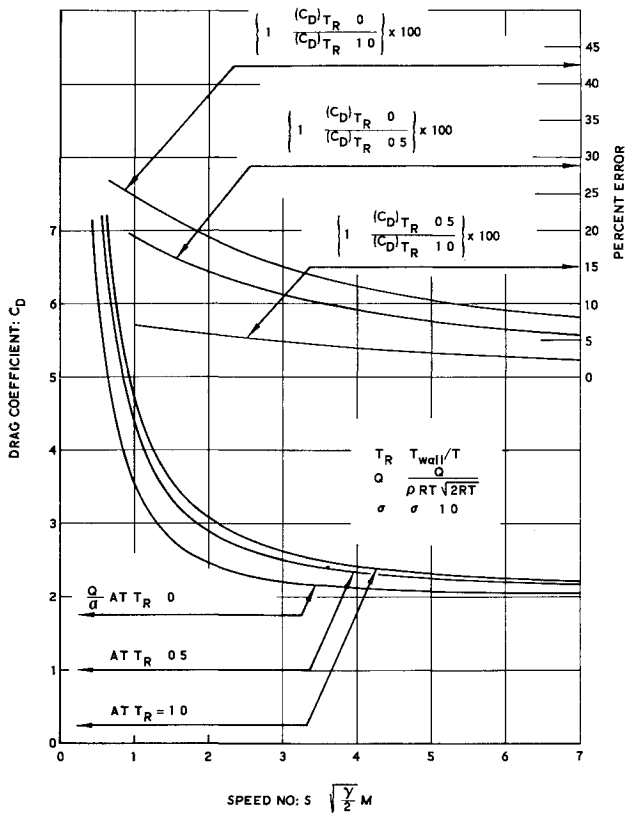

Fig 4 The effect of wall to freestream temperature ratio on sphere drag

where Q^* is a dimensionless heat-transfer parameter,

$$Q^* = Q/[\rho RT(2RT)^{1/2}] \tag{6}$$

The parameters $G(S)$ and $F(S)$ appearing in Eq (5) are functions of the speed ratio For a circular cylinder transverse to the direction of flow,

$$G(S) = \frac{e^{-s^2/2}}{\pi^{1/2}}\left[(S^2+1)\,I_0\left(\frac{S^2}{2}\right) + S^2 I_1\left(\frac{S^2}{2}\right)\right]$$

$$F(S) = \frac{e^{-s^2/2}}{2\pi^{1/2}}\left[\left(S^4 + \frac{7}{2}S^2 + 2\right)I_0\left(\frac{S^2}{2}\right) + \left(S^4 + \frac{5}{2}S^2\right)I_1\left(\frac{S^2}{2}\right)\right] \tag{7}$$

For a sphere, G and F are

$$G(S) = \frac{S}{2}\left[1 + \frac{1}{S}\,\text{ierfc}(S) + \frac{1}{2S^2}\,\text{erf}(S)\right]$$

$$F(S) = \frac{S}{8}\left\{(2S^2+5)\left[1 + \frac{\text{ierfc}(S)}{S}\right] + (2S^2+3)\,\frac{1}{2S^2}\,\text{erf}(S)\right\} \tag{8}$$

The variation of the drag coefficient with the parameters Q^*/α, T_R, and S may be calculated from the foregoing equations

Results

The effect of the thermal accommodation coefficient on cylinder and sphere drag is shown in Figs 1 and 2 These results indicate that the effect of α on C_D diminishes as the heat-transfer rate approaches zero This is not surprising, since when Q^* is equal to zero the drag coefficient is independent of α, provided that α is not zero In many practical applications the temperature ratio T_R is of the order of 0 3 — 0 5[5] At these T_R values, a small change in α changes the drag coefficient appreciably for all speed ratios, as can be seen from Figs 1 and 2 Only for high speed ratios and high temperature ratios does the effect of α on C_D become small, a condition seldom encountered in practical problems The results also indicate that for "hypothermal" free molecule flow ($S > 6$), the drag coefficient may be approximated for all values of α by

$$C_D = 2\,5 \pm 0\,5 \tag{9}$$

Equation (9) is similar to the one suggested by Schamberg in Ref 8

Q^*/α values corresponding to $T_R = 0$ and $T_R = 1\,0$ are sometimes used in the calculations of drag coefficients[6 9] The errors due to these assumptions are presented in Figs 3 and 4 It can be seen from these results that the actual T_R values should be used in calculating the drag coefficients, particularly at low speed ratios

References

[1] Bell, S and Schaaf, S A , "Aerodynamic forces on a cylinder for the free molecule flow of a nonuniform gas," ARS J **23**, 314–322 (1953)

[2] Stalder, J R , Goodwin, G , and Craeger, M O "A comparison of theory and experiment for high speed free-molecule flow," NACA Rept 1032 (1951)

[3] Stickney, R E , "An experimental investigation of free molecule momentum transfer between gases and metallic surfaces," Univ Calif , Inst Eng Res , Tech Rept HE-150-182 (1962)

[4] Wachman, H Y , "The thermal accommodation coefficient: a critical survey,"ARS J **32**, 2–12 (1962)

[5] Sentman, L H , "Effect of degree of thermal accommodation on free molecule aerodynamic coefficients," ARS J **32**, 1408–1410 (1962)

[6] Schaaf, S A and Chambré, P L , *Flow of Rarefied Gases* (Princeton University Press, Princeton, N J , 1961) Sec H 8

[7] Sauer, F M , "Convective heat transfer from spheres in a free molecule flow," J Aeronaut Sci **18**, 353–354 (1951)

[8] Schamberg, R , "Analytic representation of surface interaction for free molecule flow with application to drag of various bodies," Rand Corp Rept R-339, Sec 12 (June 1959)

[9] Stalder, J F and Zurick, V J , "Theoretical aerodynamic characteristics of bodies in a free molecule flow field," NACA TN 2423 (1951)

Initial Development of the Laminar Separated Shear Layer

ERIC BAUM*
Electro-Optical Systems, Inc , Pasadena, Calif

Introduction

SOME recent analytical studies of the compressible laminar shear layer have been based on the physical model pictured in Fig 1[1 2] The body boundary layer, separating at the rear of the body, becomes the beginning of the separated shear layer, which subsequently grows by entraining gas from the outside inviscid flow ($u = u_e$, $H = H$) and from the low-speed base flow ($u = 0$, $H = H_c$) The process of separation is characterized in this model by a discontinuous change in the inside boundary conditions from $u = 0$, $H =$

Received September 9, 1963 This research is sponsored by the Advanced Research Projects Agency, Department of Defense, under ARPA Order No 203-Al 63, monitored by the U S Army Missile Command under Contract No DA-04-495-AMC-28-(Z)

* Senior Scientist, Gas Dynamics Department, Fluid Physics Division Member AIAA

H_w, $\partial(u/u_e)/\partial Y = F_W$ (on the wall) to $u = 0$, $H = H_e$, $\partial(u/u)/\partial Y = 0$ (at the inner edge of the separated shear layer)

Of the many body boundary layer profiles for which one might wish to investigate the behavior of this model, the class of similar blowing profiles tabulated by Emmons and Leigh[3] is of particular interest because of its applicability to ablating bodies The well-developed finite difference techniques can be used for the calculation of the resulting nonsimilar separated shear layer profiles, but a singularity at the separation point caused by the discontinuity in boundary conditions makes it necessary to use a special method by which to start the calculation This paper is concerned with the development of a series solution for the velocity and total enthalpy profiles which is valid near the separation point

Sublayer Definition

After separation, distortion of the existing profile starts at the inside edge of the shear layer where the boundary condition discontinuity occurs The upper limit of the region in which the change in boundary conditions has been felt defines the extent of a sublayer which starts at the point of separation (Fig 1) Since the similar blowing velocity distributions are characterized by a region near the wall in which shear is a linear function of velocity, the approach here will be to search for a series solution of the boundary layer equations in the sublayer, with boundary conditions at the outer edge relating shear linearly to velocity Such a solution will be valid as long as the outer edge of the sublayer has not yet extended outside of the linear region of the similar blowing profile

Momentum Equation

The momentum boundary layer equation (for u_e = constant, $C = \rho\mu/\rho_e\mu$ = constant) can be written in the form[1]

$$F^{*2}(\partial^2 F^*/\partial\xi^2) + \xi^2\,\partial F^*/\partial\xi = 3S^*\xi\,\partial F^*/\partial S^* \qquad (1)$$

where

$\xi = (u/u_e)/(3S^*)^{1/3}$

$S^* = F^2_{\text{wall}}S$

$F^* = F/F_{\text{wall}}$

$S = \int_0^x C\rho\, u\, \mu\, r_0^{2k}dx$, compressible streamwise distance function

$F = \left(\frac{\partial u/u_e}{\partial Y}\right)_S$, shear function

$Y = u\, r_0^k \int_0^y \rho dy$, compressible normal distance function

F_{wall} = wall shear at separation point

$k = 0$, two-dimensional flow

$k = 1$, axisymmetric flow

r_0 = radial distance to dividing streamline

The requirement that $v = 0$ on the dividing streamline, applied to the momentum equation, results in the following expression defining the dividing streamline:

$$(\partial F^*/\partial\xi)_D F_D^*/\xi_D - \xi_D = 3S^*\, d\xi_D/dS^* \qquad (2)$$

The similar blowing profiles near the wall have the property

$$F^* \cong 1 + Bu/u_e = 1 + B\xi\,(3S^*)^{1/3} \qquad (3)$$

where $B = \dot{m}u/\tau_w$ is the blowing parameter This defines the outer edge boundary condition for the sublayer We therefore wish to find a solution to Eq (1) for small S^* with boundary conditions given by $F^*(S^*,0) = 0$ and $F^*(S^*,\infty) \to 1 + B\xi\,(3S^*)^{1/3}$; initial conditions given by $F^*(0,\xi) = 1 + B\xi\,(3S^*)^{1/3}$ After this equation is solved, the location of the dividing streamline may be found from Eq (2)

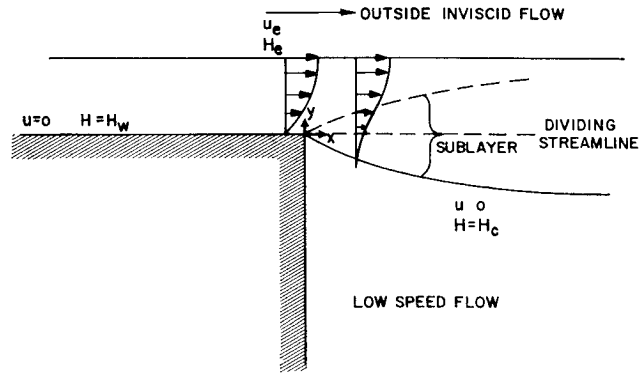

Fig 1 Separated shear layer model

Series solution

Let us assume that the shear function can be expressed as a series in powers of $B(3S^*)^{1/3}$:

$$F^*(S^*,\xi) = F^{(0)}(\xi) + F^{(1)}(\xi)B(3S^*)^{1/3} + F^{(2)}(\xi)B^2(3S^*)^{2/3} \qquad (4)$$

For convenience in satisfying boundary conditions, let $F^{(1)} = \xi + G^{(1)}(\xi)$, where $G^{(1)}$ is a new unknown function which replaces $F^{(1)}$ To satisfy the boundary conditions on F^*, we then have at the inner edge of the shear layer

$$F^{(0)}(0) = G^{(1)}(0) = F^{(2)}(0) = 0$$

and at the outer edge of the sublayer

$$F^{(0)}(\infty) \to 1$$

$$G^{(1)}(\infty) \to F^{(2)}(\infty) \to 0$$

When the series representation of the shear function, Eq (4), is substituted into the momentum boundary layer equation and terms of equal order in $B(3S^*)^{1/3}$ are collected, the resulting equations are, to the zeroth order in $B(3S^*)^{1/3}$,

$$F^{(0)2}\frac{d^2F^{(0)}}{d\xi^2} + \xi^2\frac{dF^{(0)}}{d\xi} = 0 \qquad (5)$$

and to the first order in $B\,(3S^*)^{1/3}$

$$F^{(0)2}\frac{d^2G^{(1)}}{d\xi^2} + \xi^2\frac{dG^{(1)}}{d\xi} - \xi\left(1 + \frac{2\xi}{F^{(0)}}\frac{dF^{(0)}}{d\xi}\right)G^{(1)} = \frac{2\xi^3}{F^{(0)}}\frac{dF^{(0)}}{d\xi} \qquad (6)$$

Equations (5) and (6) were solved numerically, and the results are given in Table 1 The zero- and first-order contributions to F^* are shown in Figs 2 and 3 The results are estimated to be accurate to better than three places

The zero-order solution is, of course, the exact solution for the special case $B = 0$ (corresponding to the Blasius profile on the body) This solution was previously reported in Ref 1

Dividing Streamline Location

The value of the variable ξ on the dividing streamline is now expanded in powers of $B(3S^*)^{1/3}$:

$$\xi_D = \xi_D^{(0)} + \xi_D^{(1)}B(3S^*)^{1/3} + \qquad (7)$$

Table 1 Zero-and first- order contributions to the series solution of the similar blowing boundary layer after separation

ξ	$F^{(0)}$	$G^{(1)}$	ξ	$F^{(0)}$	$G^{(1)}$
0 00	0 0000	0 0000	1 55	0 9583	−0 1709
0 05	0 0594	−0 0294	1 60	0 9650	−0 1568
0 10	0 1168	−0 0575	1 65	0 9708	−0 1429
0 15	0 1721	−0 0841	1 70	0 9758	−0 1291
0 20	0 2254	−0 1092	1 75	0 9801	−0 1157
0 25	0 2766	−0 1328	1 80	0 9838	−0 1028
0 30	0 3258	−0 1548	1 85	0 9869	−0 0905
0 35	0 3729	−0 1752	1 90	0 9895	−0 0790
0.40	0 4180	−0 1939	1 95	0 9917	−0 0683
0 45	0 4610	−0 2110	2 00	0 9935	−0 0584
0 50	0 5021	−0 2263	2 05	0 9949	−0 0495
0 55	0 5412	−0 2398	2 10	0 9961	−0 0415
0 60	0 5783	−0 2516	2 15	0 9971	−0 0344
0 65	0 6135	−0 2615	2 20	0 9978	−0 0282
0 70	0 6468	−0 2697	2 25	0 9984	−0 0229
0 75	0 6781	−0 2760	2 30	0 9989	−0 0183
0 80	0 7076	−0 2806	2 35	0 9992	−0 0145
0 85	0 7353	−0 2833	2 40	0 9995	−0 0114
0 90	0 7612	−0 2843	2 45	0 9997	−0 0088
0 95	0 7853	−0 2836	2 50	0 9998	−0 0067
1 00	0 8078	−0 2811	2 55	0 9999	−0 0050
1 05	0 8285	−0 2771	2 60	1 0000	−0 0037
1 10	0 8477	−0 2715	2 65	1 0000	−0 0027
1 15	0 8654	−0 2644	2 70	1 0000	−0 0020
1 20	0 8815	−0 2560	2 75	1 0000	−0 0014
1 25	0 8962	−0 2464	2 80	1 0000	−0 0010
1 30	0 9096	−0 2357	2 85	1 0000	−0 0007
1 35	0 9216	−0 2240	2 90	1 0000	−0 0004
1 40	0 9324	−0 2115	2 95	1 0000	−0 0003
1 45	0 9421	−0 1984	3 00	1 0000	−0 0002
1 50	0 9507	−0 1848			

Equation (2), locating the dividing streamline, becomes to the zeroth order in $B(3S^*)^{1/3}$

$$F_D^{(0)}(dF^{(0)}/d\xi)_D = -\xi_D^{(0)2} \tag{8}$$

and to the first order in $B(3S^*)^{1/3}$

$$(G_D^{(1)} + \xi_D^{(0)})\frac{\xi_D^{(0)2}}{F_D^{(0)}} + \left[\left(\frac{dG^{(1)}}{d\xi}\right)_D + 1\right]F_D^{(0)} = 3\xi_D^{(0)}\xi_D^{(1)} \tag{9}$$

When these expressions are solved simultaneously with the shear profiles $F^{(0)}(\xi)$ and $G^{(1)}(\xi)$, the solutions are found to be

$$F_D^{(0)} = 0\,611 \qquad \xi_D^{(0)} = 0\,647$$

$$G_D^{(1)} = -0\,261 \qquad \xi_D^{(1)} = 0\,394$$

$$F_D^{(1)} = \xi_D^{(0)} + G_D^{(1)} = 0\,386$$

The dividing streamline shear is given by the series expansion about $\xi = \xi_D^{(0)}$,

$$F_D^*(S^*) = F_D^*{}_{\xi=\xi_D^{(0)}} + (dF_D^*/d\xi_D)_{\xi=\xi_D^{(0)}}(\xi_D - \xi_D^{(0)}) +$$

so that

$$F_D^*(S^*) = F_D^{(0)} + 2F_D^{(1)}B(3S^*)^{1/3} \tag{10}$$

Energy Equation

When $Le = Pr = 1$, the form of the energy boundary layer equation in the Crocco coordinate system is very similar to that of the momentum equation [1] When transformed into the independent variables ξ and S^*, the energy equation in terms of the total enthalpy H becomes

$$F^{*2}\partial^2 H/\partial\xi^2 + \xi^2\partial H/\partial\xi = 3S^*\xi\partial H/\partial S^* \tag{11}$$

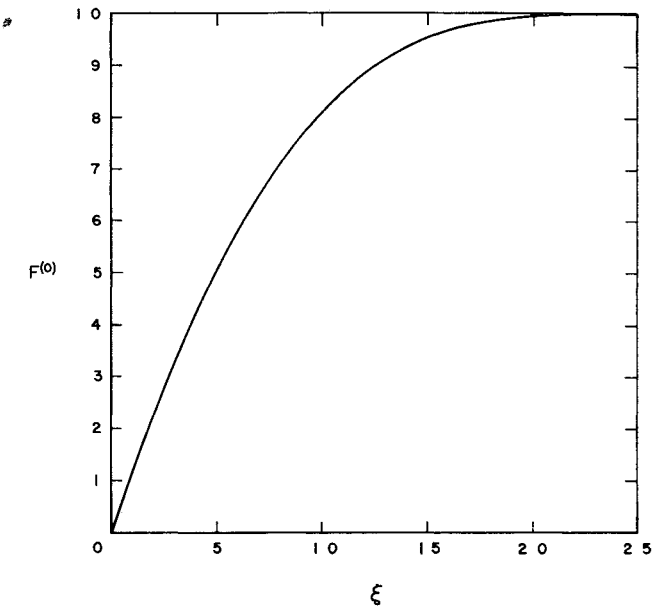

Fig 2 Zero-order contribution to solution for initial development of separated shear layer

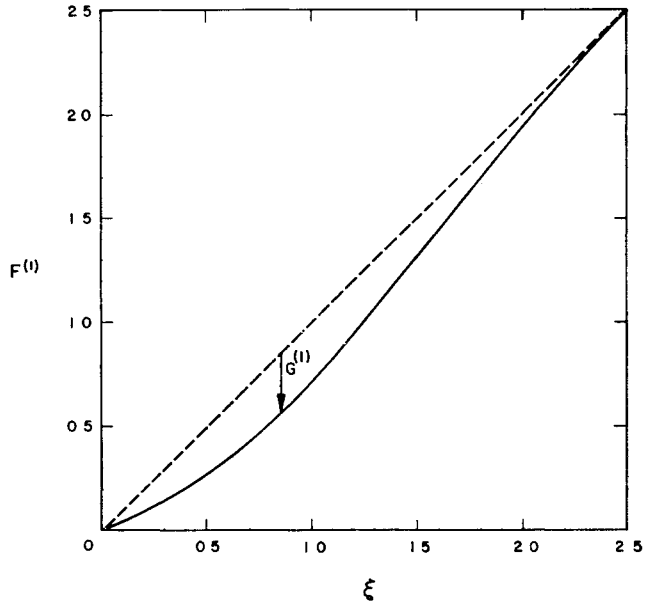

Fig 3 First-order contribution to solution for initial development of separated shear layer

with boundary conditions: $H(O,S^*) = H_c$, the total enthalpy of the low-speed gas being entrained by the shear layer (assumed constant); $H(\infty,S^*) = H$, the freestream total enthalpy Since the wall enthalpy at separation H_w is generally not the same as H_c, there is difficulty matching initial conditions unless the enthalpy is broken down into auxiliary functions Since Eq (11) is linear in H, a linear combination of functions can be used, and these can be evaluated separately The following is one of many possible ways of defining such a set of functions, here denoted by $L(u/u,S^*)$ and $W(u/u_e,S^*)$:

$$H_e - H = (H_e - H_c)L + (H_e - H_w)W \tag{12}$$

where

$$L(0,S^*) = 1 \qquad W(0,S^*) = 0$$

$$L(1,S^*) = 0 \qquad W(1,S^*) = 0$$

$$L(u/u_e,0) = 0 \qquad W(u/u,0) = (H - H)/(H_e - H_w)$$

at $s^* = 0$

When L is expanded as a series in powers of $B(3S^*)^{1/3}$, it is easily shown that the solutions for the shear profile also apply to L, that is,

$$L = 1 - F^{(0)} - G^{(1)}B(3S^*)^{1/3} \quad (13)$$

When the enthalpy in the body boundary layer is assumed to be given by the Crocco integral relation $H - H = (H - H_w)(1 - u/u)$, then $W(u/u,0) = 1 - u/u$ As shown in Ref 2, for these initial conditions $L = 1 - u/u - W$, thus reducing the number of auxiliary functions from two to one In this case the series solution for W gives

$$W = F^{(0)} - (\xi - G^{(1)}B)(3S^*)^{1/3} \quad (14)$$

The series solutions developed here are in terms of the Crocco coordinate system $[F(u/u,S), H(u/u,S)]$, but, since the location of the dividing streamline also is calculated, the normal distance coordinate Y can be evaluated by means of the integral

$$Y = \int_{u_D/u_e}^{u/u_e} \frac{1}{F}\, d\left(\frac{u}{u}\right)$$

References

[1] Denison, M R and Baum, E, "Compressible free shear layer with finite initial thickness," AIAA J 1, 342–349 (1963)

[2] King, H H and Baum, E, "Enthalpy and atom profiles in the laminar base flow," submitted to AIAA J

[3] Emmons, H W and Leigh, D, "Tabulation of the Blasius function with blowing and suction," Div Appl Sci, Combustion Aero Lab, Interim Tech Rept 9, Harvard Univ, Cambridge, Mass (1953)

Experimental Detonation Velocities and Induction Distances in Hydrogen-Air Mixtures

LOREN E BOLLINGER*

The Ohio State University, Columbus, Ohio

Detonation velocities and induction distances have been measured for hydrogen-air mixtures at 1 and 2 atm initial pressure in a 74-mm-diam, 54-m long tube The detonation velocities increase with increasing fuel concentration and with increasing initial pressure The detonation induction distances, 630–730 cm, are quite long compared to those of hydrogen-oxygen mixtures; these distances decrease at the higher initial pressure

Introduction

EXPERIMENTAL detonation velocities and induction distances have been measured for various fuel concentrations of hydrogen in air at initial pressures of 1 and 2 atm at ambient initial temperature These studies are a portion of the basic investigation of detonation phenomena which is being conducted in this laboratory Recent results have been presented in Refs 1–10

Received September 9, 1963; revision received September 26, 1963 These studies were conducted with the support of NASA under Grant NsG 44-60 with The Ohio State University Research Foundation Thanks are due R Edse for his numerous contributions made during these experiments and the interpretation of the data

* Assistant Professor, Department of Aeronautical and Astronautical Engineering, and Assistant Supervisor, Rocket Research Laboratory Associate Fellow Member AIAA

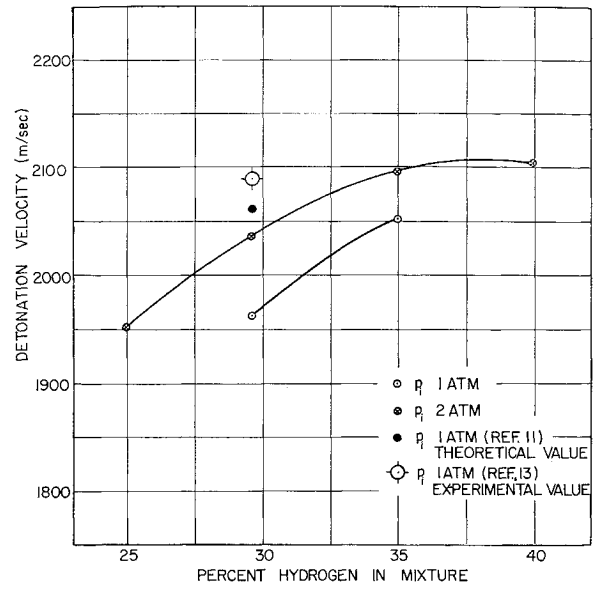

Fig 1 Experimental detonation velocities of hydrogen-air mixtures as a function of fuel concentration

These experiments were conducted in a 74-mm-i d inconel detonation tube, 54 m in length Ionization-type probes were utilized to sense the passage of the flame front Multichannel measurements of the time intervals were made with a 1-Mc chronograph system The probes have a nominal separation of 60 cm along the entire tube length Pyrofuze wire, of 0 005-in diam, was used to ignite the mixtures

A number of experiments were carried out for the same initial conditions of pressure, temperature, and fuel concentration because of the nonrepeatable nature of the flame front in the initiation region These data were averaged and graphed, including the maximum and minimum values, as a function of distance from the ignitor When the flame propagation rates became steady, the detonation velocities were determined Induction distances, the distance from the ignitor to the location in the detonation tube where the flame propagation rate first attains the detonation velocity, were ascertained from these graphs too As with previous data, two detonation induction distances are given; one distance is based on the maximum flame propagation rates and the other on average values

Discussion of Results

The velocities of the stable detonations were determined at various probe positions between 35 and 50 m from the ignitor At this distance, the detonation wave is completely stabilized for hydrogen-air mixtures as determined experimentally from measurements of the flame propagation rates along the entire length of the tube

From Fig 1 it can be seen that the detonation velocity appears to reach a maximum value near 40% fuel concentration for an initial pressure of 2 atm Data obtained at 1 atm follow the same trend as do those measured at 2 atm, but the values are somewhat lower The difference between the detonation velocities for the two values of initial pressure decreases near the maxima

It was not possible to measure detonation velocities for fuel concentrations farther from the stoichiometric value than those tabulated without making a major change in existing instrumentation The nitrogen content in the fuel-oxidizer mixture greatly decreases the flame temperature and, therefore, the degree of ionization of the product gases upon which property the present detection technique depends Special one-stage transistorized amplifiers were designed and fabricated to amplify the meager signals; without the use of these amplifiers, little of the present data could have been obtained